Bayesian operational modal analysis of Jiangyin Yangtze River Bridge

James Mark William Brownjohn
Professor of Structural Dynamics, University of Exeter, UK

Siu-Kui Au
Professor, Chair of Uncertainty, Reliability and Risk, University of Liverpool, UK

Yichen Zhu
PhD Student, University of Liverpool, UK

Zhen Sun
State Key Laboratory of Safety and Health for In-Service Long Span Bridges, Jiangsu Transportation Institute, Nanjing, China

Binbin Li
Research Associate, University of Liverpool, UK

James Bassitt
Experimental Officer, University of Exeter, UK

Emma Hudson
Research Fellow, University of Exeter, UK

Hongbin Sun
Jiangsu Yangtze Bridge Co. Ltd. Nanjing, China

Contact author: Professor James Brownjohn
CEMPS
University of Exeter
Harrison Building
Exeter EX4 4QF
E-mail: J.Brownjohn@Exeter.ac.uk
Tel: 01392-723698

Abstract

Vibration testing of long span bridges is becoming a commissioning requirement, yet such exercises represent the extreme of experimental capability, with challenges for instrumentation (due to frequency range, resolution and km-order separation of sensor) and system identification (because of the extreme low frequencies).

The challenge with instrumentation for modal analysis is managing synchronous data acquisition from sensors distributed widely apart inside and outside the structure. The ideal solution is precisely synchronised autonomous recorders that do not need cables, GPS or wireless communication.

The challenge with system identification is to maximise the reliability of modal parameters through experimental design and subsequently to identify the parameters in terms of mean values and standard errors. The challenge is particularly severe for modes with low frequency and damping typical of long span bridges. One solution is to apply 'third generation' operational modal analysis procedures using Bayesian approaches in both the planning and analysis stages.

The paper presents an exercise on the Jiangyin Yangtze River Bridge, a suspension bridge with a 1,385m main span. The exercise comprised planning of a test campaign to optimise the reliability of operational modal analysis, the deployment of a set of independent data acquisition units synchronised using precision oven controlled crystal oscillators and the subsequent identification of a set of modal parameters in terms of mean and variance errors.

Although the bridge has had structural health monitoring technology installed since it was completed, this was the first full modal survey, aimed at identifying important features of the modal behaviour rather than providing fine resolution of mode shapes through the whole structure. Therefore, measurements were made in only the (south) tower, while torsional behaviour was identified by a single measurement using a pair of recorders across the carriageway. The modal survey revealed a first lateral symmetric mode with natural frequency 0.0536 Hz with standard error ±3.6% and damping ratio 4.4% with standard error ±88%. First vertical mode is antisymmetric with frequency 0.11 Hz ± 1.2% and damping ratio 4.9% ± 41%.

A significant and novel element of the exercise was planning of the measurement setups and their necessary duration linked to prior estimation of the precision of the frequency and damping estimates. The second novelty is the use of the multi-sensor precision synchronised acquisition without external time reference on a structure of this scale. The challenges of ambient vibration testing and modal identification in a complex environment are addressed leveraging on advances in practical implementation and scientific understanding of the problem.

Highlights

Ambient vibration test on 1385 m Jiangyin Yangtze River Bridge, by western academics.

Application of uncertainty laws of Bayesian operational modal analysis for test planning with and without preliminary data.

Bayesian operational modal analysis of acceleration data, including challenging lateral vibration modes

Design and use in the field testing of precisely synchronised loggers not relying on GPS or wireless.

Keywords: Bayesian operational modal analysis suspension bridge uncertainty synchronisation

1 Introduction

Ambient vibration testing (AVT) is becoming an indispensable tool for managing the performance of large scale civil infrastructure where forced vibration testing is logistically infeasible. However there are specific challenges to AVT in particular for long span and tall structures in both the experimental art and the subsequent analysis of response time series. This paper describes advances in both technologies aimed at improving the effectiveness of experimental AVT campaigns to provide the most reliable estimates of modal parameters (MP) with the least experimental cost and which are applied together on an exemplar study, Jiangyin Yangtze River Bridge ('Jiangyin Bridge'), a suspension bridge with a 1,385 m main span in Jiangsu Province, China.

1.1 Motivation for managing uncertainty of modal parameter (MP) estimates

Knowledge of structural modal parameters or MP (for both singular and plural form) representing modal frequencies, damping ratios, shapes and masses is a fundamental requirement for design against dynamic loads (wind, earthquake, human excitation). MP estimation is central to finite element model updating and the dependent performance simulations. It has long been recognised as an effective means for uncertainty mitigation in structural dynamics [1] and is a vital prerequisite for:

- Vibration control devices [2]: Design and maintenance of effective tuned mass dampers depends on precise knowledge of modal damping and frequency;

- Retrofits [3]: If the retrofit aims to improve vibration serviceability, both design and evaluation of the retrofit depend on reliable MP estimates;

- Structural Health Monitoring (SHM) systems [4]: MP (e.g. frequencies) are classic indicators of structural state so the ability to identify and statistically qualify small changes will enhance SHM system utility for tracking structure condition through shifts and drifts in MP.

Computer models of tall buildings often grossly misrepresent the as-built characteristics, which is evidenced by measured MPs significantly differing from predictions [1]. A specific example is the 280 m Republic Plaza building in Singapore where >0.19 Hz fundamental mode frequencies measured by AVT indicated almost doubled as-built stiffness compared to a design estimate of 0.14 Hz [5]. Such conservatism and over-design is not sustainable and needs to be tempered by experience from AVT.

For damping, other than for discrete damping elements [6,7] available models are all empirical. Values used in design are based on historic databases [6,8] distilled in codes of practice [9], and usually derived from response using '1st generation' operational modal analysis (OMA) techniques (e.g. random decrement, half-power bandwidth) [10] having questionable reliability. Building occupants pay a premium for high-rise comfort and to be sure of avoiding poor vibration serviceability and loss of revenue amidst uncertainty in inherent structural damping, vibration control devices may be specified. These are expensive and use premium space. For long span bridges flutter speeds increase with damping. Unlike computational underestimation of natural frequency, experimental estimates of damping are usually high so that safety margin is also overestimated.

MP identification using forced vibration testing (FVT) with controlled input (force) [11] is believed to produce the most reliable MP estimates. However, FVT is only feasible for automotive/aerospace applications (such as ground vibration testing) and relatively small civil structures such as footbridges and floors having modal masses with maximum order 10^3 tonnes and natural frequencies usually above 1 Hz. For long span and tall structures having modal frequencies of the order 0.1 Hz and modal masses usually upwards of 10^4 tonnes, artificial forcing is logistically infeasible. Therefore, AVTs providing response data for OMA have become the standard investigation tool.

A trend in AVT for structural commissioning tests (e.g. Burj Khalifa and Queensferry Crossing) to corroborate design assumptions has accelerated with sophisticated '2nd generation' OMA techniques such as stochastic subspace identification (SSI) and frequency domain decomposition (FDD) [12,13]. However, the problem remains that absence of input loading data in AVT leads to fundamentally much higher MP estimate variability and lower repeatability compared to FVT. This uncertainty is well recognised [8,14] but there has been no quantitative account for its origin, nor any quantitative guideline for test configuration (sensor location, load intensity, signal/noise ratio (SNR) and measurement duration) to achieve a desired identification precision. Recent ASCE guidance [1] states that prediction of structural (dynamic) properties is more of an art than a science; there are few reliable measurements of structural damping and values used in performance predictions are generally 'crude and simplified estimates'.

With aero-elasticity a major factor in long span bridge performance at ultimate limit state, designers rely heavily on damping estimation from existing prototypes via AVTs that have had poor uncertainty management. Existing databases [6,8] of field-identified tall building damping values used for design show great scatter with no information on their reliability [15,16] and there is still no commonly accepted amplitude-dependent damping model for even the simplest building configuration. For the tallest buildings vibration serviceability, which depends critically on first mode frequency and damping, governs design, and reliable performance data are both scarce and critically important. For long span bridges, collections of damping data [17][18] are rarer and older.

1.2 Uncertainty laws for Bayesian OMA

Due to the accepted reliability of MP estimation using forced vibration testing, there are few studies on accuracy [19], while there are presently several techniques dealing with reliability of OMA, particularly for SSI [20–23], including a commercial implementation. Uncertainty quantification is central to '3rd generation' Bayesian OMA methods [24] that adopt a radically different philosophy to 1st and 2nd generation OMA methods by posing the question 'what is known about MP based on the given data?'. Answers are expressed via the *posterior* probability density function (PDF) of MP (θ) for given response data (D) implied fundamentally using Bayes' theorem [25] i.e. $P(\theta|D)$. The covariance matrix associated with the posterior PDF then naturally quantifies the identification uncertainty of MP for the given data set and modelling assumptions. This is in contrast to non-Bayesian methods where the uncertainty refers to the estimates of the MP rather than the MP themselves, and is 'inherent' in nature, i.e. does not depend on data.

Even so, algorithms for calculating uncertainty, be they Bayesian or non-Bayesian, only allow MP uncertainty to be calculated in a 'point-wise' manner (i.e., 'what') for given data, which yields little or no understanding about uncertainty (i.e., 'why'). Therefore, the main aim of the 'BAYOMALAW' research project [26] funded by the Engineering and Physical Sciences Research Council has been to deliver 'uncertainty laws' using Bayesian inference to express MP uncertainties explicitly as functions of test configuration (measurement noise, environmental load intensity and sensor configuration) so that MP uncertainty can be prescribed and managed [27]. The project has aimed at providing a quantitative account for the origin of uncertainty along with quantitative guideline for test configuration to achieve a desired identification precision. The exercise reported here is an early application.

Figure 1 provides an outline of the research. (Conventional) efforts on Bayesian OMA algorithm development belong to the central (unshaded) part of the figure. Uncertainty law research is concerned with the shaded parts that address the challenge of understanding identification uncertainty and mastering its relationship with test configuration. Previous experience in the ambient modal identification research community has led to advice on best practice for reliable MP identification [28]. Following a Bayesian approach, this has been formalised [29][30] in the form of 'zeroth order laws'. These are closed form expressions for MP uncertainty (variance) derived assuming sufficiently long data with high SNR, analogous to the Laws of Large Numbers in classical statistics. Accounting only for zeroth order effects, they link MP identification precision with data duration and frequency domain resolution of spectral peaks in the case of well-separated modes identified using data from a single configuration of sensor location and type (or setup). The research was later extended [27] to include 'first order effects', where test configuration starts making influence through the 'modal SNR' (see equation (2) later). The zeroth and first order laws are presented in section 4.

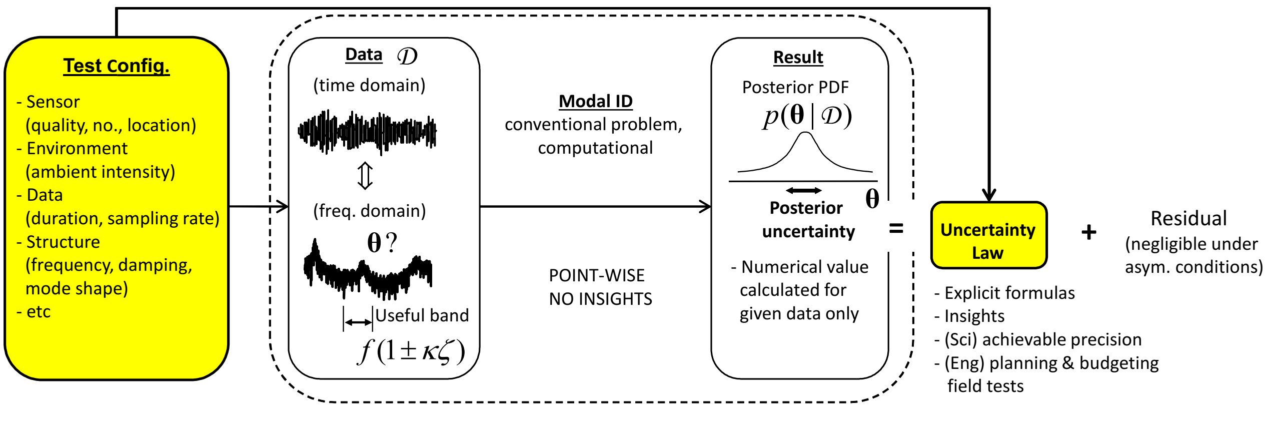

Figure 1: Objective of BAYOMALAW project

A secondary aim of the project, in support of the uncertainty management, is the creation of a bespoke instrumentation system that simplifies the experimental work by removing the requirement to use wires, radio transmission or GPS for synchronising data among accelerometers separated by distances of the order of 1 km. This is achieved using high precision acquisition clocks and robust data acquisition architecture.

The project combines theoretical development with experimental trials and verification in a number of steps, beginning with the effects of modal SNR. Modal SNR is a key parameter that quantifies test configurations such as measurement noise, environmental load intensities and the measured degrees of freedom.

The large-scale experimental application and test of BAYOMALAW methodology focused on the 1,385 m span Jiangyin Bridge, with phases of preparation, on-site measurement and then post-processing. The phase of preparation included

- development of precision synchronised autonomous acceleration recorders developed as bespoke improvement on the technology used for ambient vibration testing of the Humber Bridge in 2008 [31] and
- obtaining sample data from the structural health monitoring system operated by Jiangsu Transportation Institute (JSTI). The data were used to evaluate expected SNR and the strategy of reference and rover positions, as well as for defining measurement setup duration.

The testing phase involved three days of vibration measurements carried out by a team from JSTI, the University of Liverpool and the University of Exeter. Finally, the post-processing phase to recover MP and their uncertainties was carried out by researchers from the University of Liverpool.

Hence the paper first describes the bridge, then development of the autonomous loggers. Next the sample data and test planning are described. The field measurements are then summarised and the MP estimates presented. Finally, the implications for future studies and next steps are defined.

2 Jiangyin Yantze River Bridge

Jiangyin Bridge (Figure 2) with a single span of 1,385 m carries the G2 expressway across the Yangtze River in Jiangsu province, China, approximately 160 km northeast of Shanghai. It was the world's fourth longest span when completed in 1999. The 0.876 m diameter main cables each support the deck via 85 pairs of vertical hangers and are formed by prefabricated parallel wire strands, each constructed from 127 × 5.35 mm diameter galvanised steel wires with 1,600 MPa tensile strength. Back stays attached to large gravity anchorages carry no deck load and have a diameter of 0.897 m. Towers with a height of 190 m are portal frames created by two hollow tower columns of reinforced concrete and three transverse beams. The main girder is a streamlined box section with a width of 36.9 m and a height of 3 m carrying a 29.5 m wide deck with three lanes of cars, buses and trucks in each direction. There is a 1.8 m walkway each side with limited access, for maintenance purposes.

Figure 2: Jiangyin Bridge

Information on the design and construction is provided in [32] and an elevation view is provided in Figure 3.

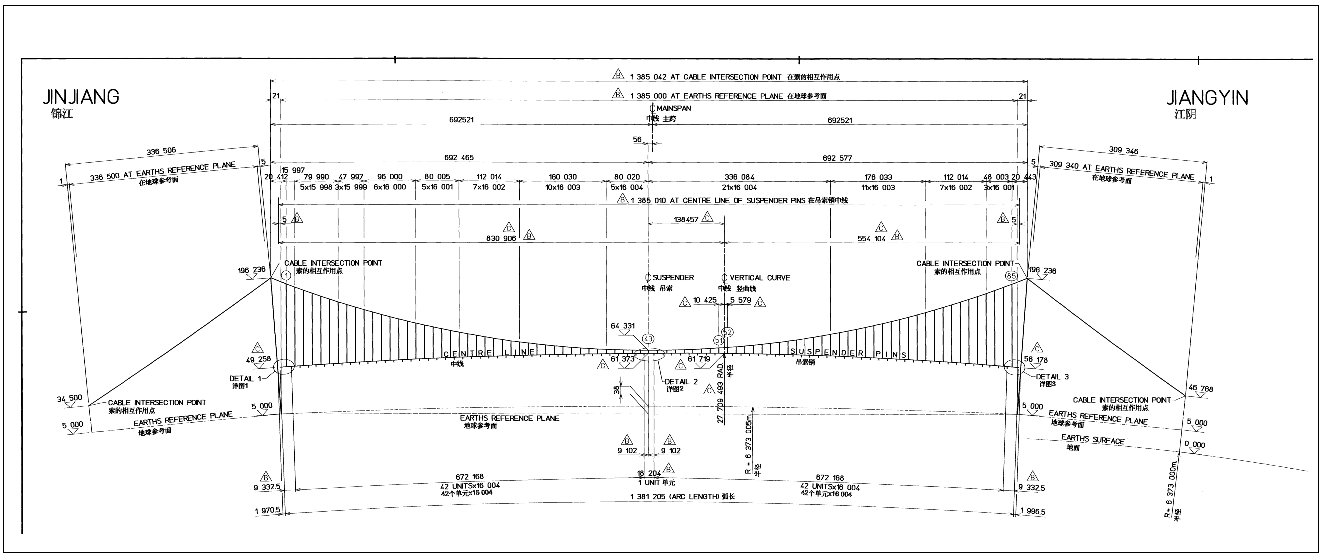

Figure 3: Jiangyin Bridge elevation

A structural health monitoring (SHM) system was installed at the time of construction but was upgraded in 2005 [32] to comprise 116 fibre Bragg gating sensors for strain and temperature measurement, 35 uniaxial accelerometers, nine GPS receivers and four displacement sensors. Relevant for the present study, 15 of the uniaxial accelerometers are located in the girder, at the 1/8, 1/4, 3/8 1/2 and 3/4-span distances from the north tower and GPS receivers are mounted on rigid posts at 1/4, 1/2 and 3/4-span locations on the east and west sides of the roadway.

While SHM system data have been extensively analysed [32,33], there is no information available on modal properties other than a Chinese language report [34] referring to GPS and acceleration data from the SHM system. For lateral vibration a symmetric mode at 0.0546 Hz and an antisymmetric mode at 0.1314 Hz were identified from accelerometer data, while for vertical vibrations an antisymmetric mode at 0.0891 Hz and a symmetric mode at 0.1258 Hz were identified. The identification algorithm is not known.

One specific concern with Jiangyin Bridge is the behaviour of the expansion joints located at each end of the main span. These were replaced in 2007 due to damage, and movement has been controlled using large viscous dampers [35] installed at the same time, so it is possible that these may affect the dynamic behaviour of the bridge.

3 Logging systems for long span bridge ambient vibration testing

3.1 Previous instrumentation deployments for long span suspension bridges

Previous experience in ambient vibration tests (AVTs) on long span bridges had considerable bearing on the design of bespoke instrumentation for Jiangyin Bridge AVT and subsequent deployments.

In the 1980s, AVTs on:

- Humber Bridge [36], with main span 1,410 m and suspended sidespans of 280 m and 530 m.
- 15 July Martyrs Bridge, also known as First Bosporus Bridge, and referred to here as B1 [37] and
- Fatih Sultan Mehmet Bridge, also known as Second Bosporus Bridge and referred to here as B2 [38]

used small wired arrays comprising a fixed reference accelerometer and no more than four roving accelerometers and used 1st generation methods for OMA. Up to eight signal cables (250 m each) were laid inside the box girder and daisy-chained to reach accelerometers that could be up to 1 km from the location of the reference sensor and acquisition system. A four-channel analog tape recorder with poor signal to noise ratio was used to record acceleration data that were post-processed by replaying signals through a two-channel spectrum analyser, one pair at a time. These AVTs took up to 10 working days covering a sufficient number of degrees of freedom using available cables and sensors while trying to obtain recordings of approximately one hour per measurement. B1 (1,074 m main span) and B2 (1,090 m main span) do not have suspended side spans which simplified the measurements, but for each of the three bridges considerable trouble was taken to measure at several locations in both pylons of both towers.

An AVT of the Tamar Bridge, which has a 335 m main span was carried in 2006 [39]. Being a much shorter bridge, it was possible, thanks to good weather and strong support from the bridge management team, to do the test in a single day, but with some limitations. First, the bridge has a truss girder which is very difficult to negotiate so it was possible only to work outside the bridge, placing accelerometers on flat spaces between the walkway and south traffic lanes. It was also possible (with some difficulty) to carry two signal cables under the road deck, through the truss to the north side to be used as reference sensors opposite two sensors on the south side. Second, a limited number of 100 m signal cables was available.

To compensate for restrictions, best practice available for planning measurements to be used for OMA (now formally outlined in [28]) was followed. This defines the minimum number of cycles of the vibration mode to be identified as $10/\zeta$, so that assuming the same damping, the higher modal frequencies (shorter periods) allowed shorter recordings, as little as 15 minutes. Also a high specification 24-channel data acquisition system with a full set of accelerometers allowed for the simultaneous recording of 16 acceleration signals. Accelerometers were roved only along the south side of the bridge and only at the upper portal of the north pylons, allowing for a much more efficient measurement campaign. A 2nd generation OMA was used, resulting in a rapid evaluation of the MP, and helping to identify modes that were subsequently tracked in real time by a permanent SHM system [40] using automated and optimised OMA.

The Humber Bridge was retested in 2008 [31] in collaboration with researchers from the Faculty of Engineering of the University of Porto (FEUP) and from City University of Hong Kong. The campaign took advantage of the FEUP AVT technology that used GeoSIG autonomous recorders with GPS-synchronised acquisition. Combining resources provided a set of ten recorders each running a triaxial accelerometer set. Two pairs of recorders acted as rovers (two span-wise locations, one recorder each side of the deck on the walkway) leaving three pairs to rove all other span-wise locations, as well as all pier and portal levels of both towers' accelerometers channels (76 locations), doubling the level of detail in the 1985 test. Apart from measurements at mid-portals levels in the towers with no exterior access, all measurements used recorders on or outside the bridge, ensuring good reception by GPS antennae and enabling faster relocation of roving accelerometers between measurements. With this level of instrumentation it was possible to finish the AVT within five days which was followed by OMA using a range of 2nd generation procedures. One problem that surfaced during the OMA was the imperfect synchronisation of recorders. Errors of up to 7 ms were identified for units with GPS line of sight, more so for recorders inside the tower without the GPS satellite visibility.

3.2 Instrumentation for Jiangyin Bridge AVT: the OCXO loggers

The experience described above clearly indicated that the most efficient and effective data acquisition system for an AVT of a long span bridge would comprise autonomous recorders such as the GeoSIG recorder units. Concerns about synchronisation accuracy and the need to operate inside or outside a structure without any requirement for wired or wireless communication led to a specification for autonomous recorders with highly accurate clocks that would maintain synchronisation to better than 1 ms during a day of recording. There are two problems to address, the first being how to start a recording across a set of data *loggers* using a common timebase, the second being how to minimise drift due to acquisition timing variations.

3.2.1 Logger design

In principle, a common timebase could be set using GPS [41], but standard crystal oscillators controlling data acquisition hardware such as the popular National Instruments NI 9234 have quoted internal master timebase accuracy 50 parts per million (ppm) maximum. This means that a pair of initially synchronised but separate units could, in the worst case scenario, have timebases different by 0.36 s after just one hour of operation.

The best precision quartz oscillators available quote an accuracy of no better than 5 ppm, while oven controlled crystal oscillators (OCXOs) offer precision better than 1 ppm. Oscillator quartz crystal frequencies vary because of stiffness dependence on temperature, and OCXOs precisely control the oscillator temperature using a small oven. The technique of using OCXOs to maintain synchronisation became available in proprietary systems e.g. [42] but a system was required with complete flexibility e.g. to work with available triaxial or uniaxial accelerometers. Therefore, a set of autonomous loggers was built around National Instruments (NI) compact acquisition units controlled by 10 MHz OCXOs.

Each data logger, in a waterproof case, comprises power supply modules, switching and connectors as well as a 4-slot CompactRIO cRIO-9064 embedded controller. Each cRIO-9064 controls a 24-bit four channel NI 9234 vibration input module set to acquire ±5V. To achieve the sub-1 ppm synchronisation a blank NI 9977 C-series module is used to house the OCXO while a NI-9402 high speed digital IO module monitors the 'local' OCXO clock ticks at 120 MHz. The cRIO-9064's integrated FPGA (programmed in LabVIEW environment) drives the acquisition module at its maximum 51.2kHz, then decimating the acquired signals based on the local OCXO clock ticks, after appropriate filtering to avoid aliasing issues.

One logger is programmed as a master, the remaining loggers as slaves. To start synchronisation, the master unit is first powered up (using a battery or mains supply), followed by each of the slave loggers. Once the master is running and acquiring data (indicated by an LED flash sequence) the clock signal containing timing information from its master OCXO is briefly connected to the OCXO inside each of the slave units by BNC cable. The slave OCXO updates its own timing information so that the two clocks are synchronised. When the master OCXO has been connected to each slave (the process takes a few seconds and is confirmed by a flashing LED sequence) all loggers are then operating with the same timebase.

Using high-speed direct memory access, all acquired vibration/acceleration data are streamed to technical data management (TDMS) files stored on a high-capacity USB drive in the cRIO-9064. The data can be accessed during measurement via Ethernet to check data streams and to retrieve stored data using FTP. Alternatively each USB drive can be removed to copy files directly to the analysis PC.

When powered by batteries the loggers can then be spatially distributed. Each logger is set to work with either a set of Honeywell QA-750 uniaxial accelerometers or a single Japanese Aerospace JA-70SA triaxial accelerometer; Figure 4 shows a set of four synchronised loggers using battery power and acquiring from JA-70SA accelerometers. The LabVIEW application to check data acquisition during operation, is being used on the laptop in the setup shown in Figure 4.

The measurement duration depends on the test plan, logistics and ultimately battery capacity. NI hardware and OCXO together draw 7 W so planned battery capacity has to be more than adequate for a day of site measurement that can potentially last up to 12 hours. In fact a more compact but lower capacity battery can be installed in the yellow box, but could only be used if the boxes are shipped to site by road or rail, due to civil aviation restrictions on carrying batteries which work against any battery operated system.

When all measurements are complete, the loggers are turned off, USB drives removed and data transferred to a prepared set of directories on the PC. A MATLAB script is used to assemble data into a common time-synchronised set covering the common period of logger operation and the data file is chopped into pieces representing individual measurements. This part of the operation is low-tech, requiring written records of time and location for each logger.

Figure 4: Using a set of four OCXO-controlled loggers with JA-70SA triaxial accelerometers.

3.2.2 Logger performance: noise floor and synchronisation drift

The logger system was function-tested using a field test on a 100 m cable-stayed footbridge in Exeter [43] shortly before the equipment was shipped to Shanghai for the Jiangyin Bridge AVT. In addition the noise floor of the system was evaluated using a 'huddle test' [44] which is a common recording of collocated sensors and loggers that isolates sensor noise by removing the common true structural vibration. Figure 4 shows preparation for the huddle test using the JA-70SA accelerometers planned to be used at Jiangyin Bridge. Due to an operational problem with the JAs (subsequently resolved) QA-750 accelerometers were in fact used, and the noise floor was separately evaluated in set up similar to Figure 4.

The huddle test is based on the discovery [45] that no more than three channels of data from three identical and collocated sensors can be used to identify their noise floor. For a single sensor, noise floor evaluation would require either an extremely quiet environment (e.g. in a salt mine) or some form of isolation [45] but using the minimum of three sensors allows redundant information about the mechanical excitation of the collocated sensors to be removed from their signals.

Figure 5 shows the procedure applied to 14 hours of vertical acceleration data from QA-750 accelerometers connected to three (separate) loggers. The logarithmic axes emphasise the relatively high noise at low frequencies common to all types of accelerometer. Based on the plot, a conservative estimate of self-noise of sensor and analog to digital converter at 0.05 Hz (where the first lateral mode is expected) is 30 $\mu ms^{-2}/\sqrt{Hz}$ i.e. 3 $\mu g/\sqrt{Hz}$. This noise floor was used in the test planning described in 4.2.

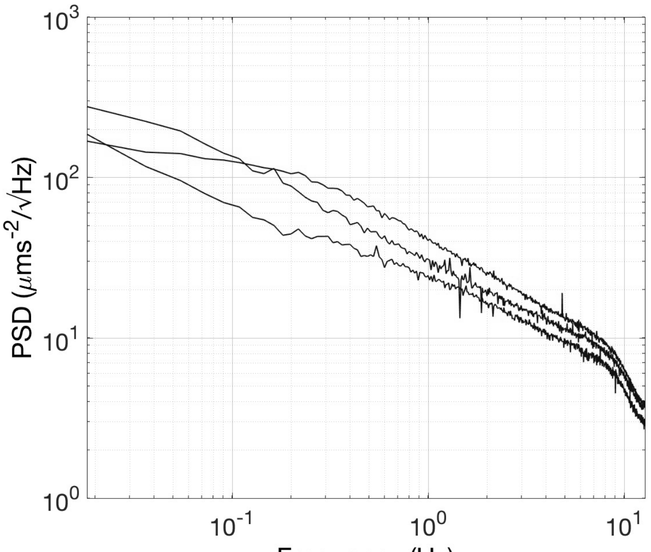

Figure 5: Power spectral density (PSD) of QA-750 noise floor from Huddle test of Figure 4, using [45].

A check in synchronisation drift was required because the resulting phase angle shift between channels could compromise MP identification. The four loggers were sat on a laboratory floor, synchronised and left for 42 hours to record ambient vibrations including weak response of the floor to footfalls. Data samples were taken from the recording after three hours and 42 hours and cross-power spectra evaluated. Transfer functions were constructed for three slave loggers with respect to the master, and Figure 6 shows phase angle for one of the slave loggers (relative to the master logger) for around 6 Hz, which is the first mode frequency of the floor.

Consider that the common signal in a recording sample should result in the same Fourier amplitude $Asin(\omega t + \phi)$ at a given frequency ω having a common phase angle ϕ that depends on the starting angle of the sinusoid at $t = 0$. Any difference in phase angle among signals recorded by different loggers must be due to a different local value *t* at the start time of the sample so that synchronisation drift $\Delta t = \phi/\omega$.

The slope at 3 hours is approximately 10°/Hz i.e. 0.1745 radian per 2π radian/s. This is $\Delta t = 0.028\ s$ drift in 10,800 s i.e. 2.6 ppm. After 42 hours the phase shift is 126°/Hz corresponding to $\Delta t = 0.35\ s$ i.e. 2.3 ppm. This indicates a drift that is approximately linear with time, and this varies between loggers. The implication is that the phase shift for 1 Hz mode after 10 hours of operation would be at a maximum of 30°.

To avoid compromising OMA procedures that are sensitive to phase angle this drift be fixed by resampling signals in post-processing if the drift is known.

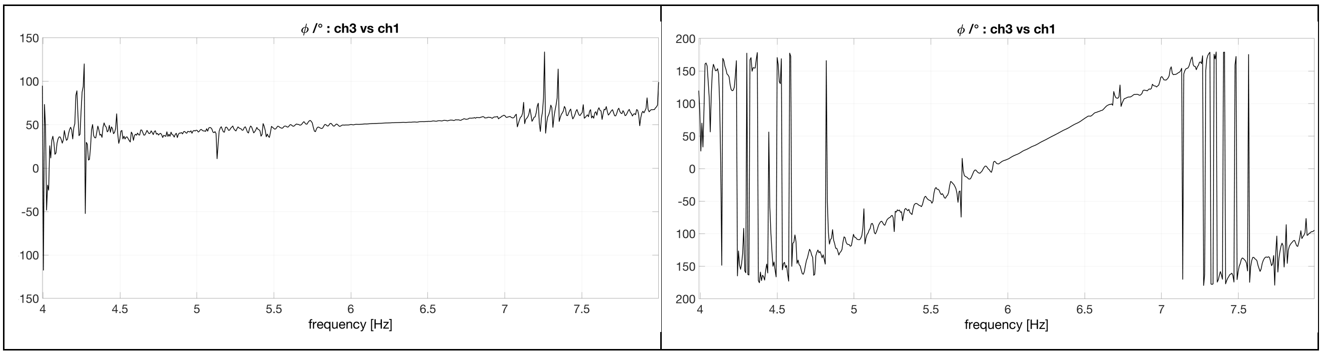

Figure 6: Effect of synchronisation drift on phase angle after a) 3 hours and b) 42 hours.

While the OCXO clocks are expected to have minimal drift, an explanation of the observed drift is that actual clock speeds could apparently differ slightly from the nominal 120 MHz. To check this, the loggers OCXOs were transplanted into GPS-synchronised wireless sensor nodes [41] to test the clock speed. Due to lack of time between logger construction and deployment in China, both this study and the 42 h recording followed the field test, and the actual clock speeds for the four deployed OCXOs are shown in Figure 7. The plot indicates that clocks need a short warming-up period period to reach a stable frequency which is maintained to within 0.2 ppm for a long duration. Even though individual clock speeds are stable, the set of four speeds shows significant variance.

The OCXOs have been replaced with units having tighter clock speed tolerances and shorter times to warm up. The replacement OCXOs which will be used in a larger set of ten loggers reach the stable frequency faster and limit aggregate drift to 0.4 ppm.

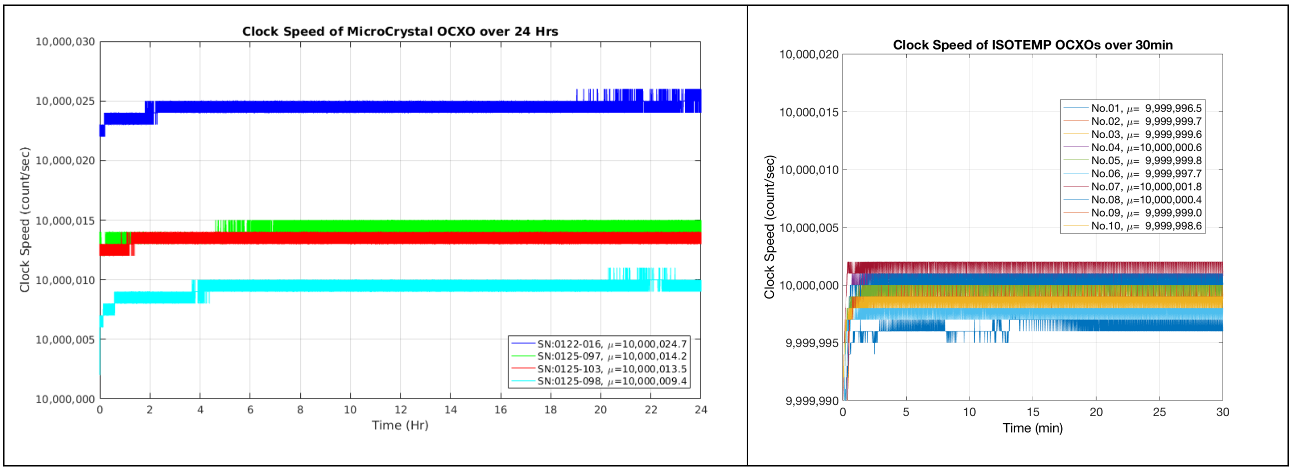

Figure 7: OCXO clock speeds for two types of OCXO (left) for four units used at Jiangyin Bridge and (right) for ten units used subsequently.

4 Planning using BAYOMALAW

Planning for the Jiangyin Bridge modal test was based on a combination of prior experience with other bridges and preliminary data for Jiangyin Bridge obtained by JSTI.

In a Bayesian context, the identification uncertainty is quantified in terms of its variance given information of the data set, but the value itself (for the given set of data) reveals little insight about how it depends on the quality or statistical characteristics of data. Beyond the ability to *calculate*, planning ambient vibration tests requires the ability to *understand* identification uncertainty and master its relationship with test configuration. When the data indeed follow the distribution assumed in the identification, i.e., stochastic stationary and classically damped, it can be shown that the variance follows a statistical law analogous to the Laws of Large Numbers in classical statistics. It has a deterministic part and a random part. The random part depends on specific details of the data and is asymptotically negligible as data length increases. The deterministic part depends on the 'information content' of the data that is related to test configuration and is what affects test-planning decisions. This deterministic part is referred to as uncertainty laws in recent studies [27,29].

The OMA uncertainty laws are closed form asymptotic expressions and they are the primary scientific target of the BAYOMALAW project. The derivation involves asymptotics and leverages on the particular mathematical structure of the OMA problem in specific contexts such as well-separated modes, closely-spaced modes, multiple setups, but the findings to date show that the results can be remarkably simple [29]. The findings can be used to guide test planning for different circumstances of prior information.

4.1 BAYOMALAW for planning with preliminary data

When the preliminary data are available, their quality can be assessed using their power spectral density (PSD), and the identification uncertainty of the MP can then be quantified using 'zeroth order' relationships with e.g. data duration [29][30] corrected for 'first order' effects [27] due to test configuration. The uncertainty laws are developed for modal frequency, damping and shape.

Of these, damping ratio is the parameter whose uncertainty is simultaneously the most important and hardest to control. For well-separated modes, small damping and long data in a single measurement, or setup using one or more response data channels the posterior CoV. δ (coefficient of variation = standard deviation/mean) for damping ratio is asymptotically given by

$$\delta \sim \delta_1 = \delta_0 \sqrt{1 + \frac{a(\kappa)}{\gamma}}. \quad (1)$$

'~' means 'asymptotic to' and denotes that CoV. δ tends to δ_1 asymptotically as $\zeta \to 0$, and data length→∞. Here, δ_0 and δ_1 represent the CoVs, respectively, given by 'zeroth order' and 'first order' uncertainty laws.

The parameter of particular relevance is the modal SNR γ, whose definition is motivated from the uncertainty law theory. Defining S as the 'modal force PSD', the modal SNR is the ratio of modal PSD $S/4\zeta^2$ to the noise PSD S_e at the natural frequency f i.e.

$$\gamma = \frac{S}{4 S_e \zeta^2} \quad (2)$$

while the zeroth order law that gives δ when the modal SNR is infinite [29,30] is given by

$$\delta_0 = \frac{1}{\sqrt{2\pi\zeta N_c B(\kappa)}}. \quad (3)$$

N_c is the 'effective data length' expressing the data duration T as a multiple of the natural period $1/f$, i.e.

$$N_c = Tf \quad (4)$$

and is conventionally understood to be a key parameter controlling reliability of MP obtained from OMA.

κ is a dimensionless 'bandwidth factor' that reflects usable bandwidth $f(1 \pm \kappa\zeta)$ around the natural frequency f and on which depend parameters $a(\kappa)$ and $B(\kappa)$:

$$B(\kappa) = \frac{2}{\pi}\left[tan^{-1}(\kappa) + \frac{\kappa}{\kappa^2+1} - \frac{2}{\kappa}(tan^{-1}\kappa)^2\right] \quad (5)$$

$$a(\kappa) = \frac{4(\kappa^2+1)(3tan^{-1}\kappa - 3\kappa + \kappa^2 tan^{-1}\kappa)tan^{-1}\kappa}{3[(\kappa^2+1)(\kappa - 2tan^{-1}\kappa)tan^{-1}\kappa + \kappa^2]}. \quad (6)$$

Figure 8 plots $B(\kappa)$ and $a(\kappa)$, which are both increasing functions of κ.

$\kappa = 1$ represents the classical 'half power bandwidth' containing $2\zeta N_c$ FFT points [18] and T can be considered to be long when the number of FFT points $N_f = 2\kappa\zeta N_c$ is large compared to 1.

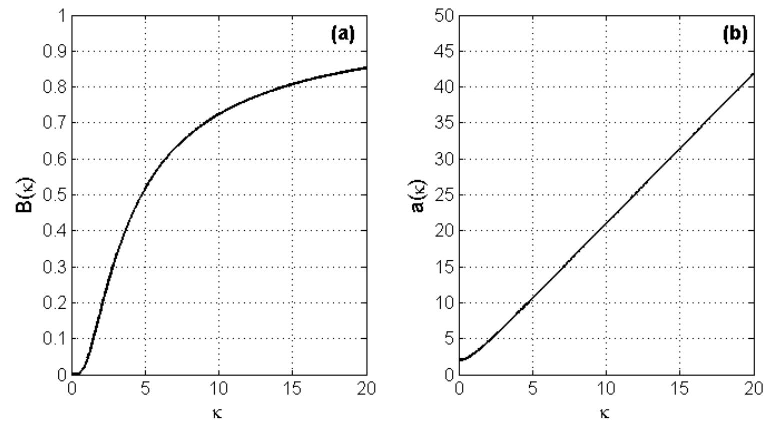

Figure 8: Plot of $B(\kappa)$ (a) and $a(\kappa)$ (b) with bandwidth factor κ.

The zeroth order uncertainty law δ_0 gives the achievable identification precision because it is the lower limit of uncertainty for ideal situation with noiseless equipment ($\gamma \rightarrow \infty$). This limit is not zero because the (input) ambient excitation is unknown. The zeroth order law is less informative in guiding the ambient vibration test because the effect of modal SNR γ has not been explicitly captured. The first order uncertainty law δ_1 depends on the modal SNR, thus providing a key quantity for planning the ambient vibration test.

A sample of data from the Jiangyin Bridge SHM system was provided by JSTI but proved to be problematic in terms of the synchronisation and orientation of the sensors. However the data were sufficient to indicate a vertical mode at 0.106 Hz with a damping ratio of 4 % and a usable identification band of [0.07 0.11] Hz that gives a bandwidth factor 4.78. Figure 9a shows that for 15% CoV., N_c=360 natural periods are required, corresponding to one hour for the given mode.

From the preliminary data, it is estimated S=9×10^{-8}g^2/Hz and S_e=5.3×10^{-7}g^2/Hz. Using the 4% damping estimate for the first vertical mode provides an estimated SNR=27 using equation (2). This SNR leads to a 20% increase (compared to ideal noiseless situation) using the first order correction (Figure 9b). The ambient excitation S cannot be directly controlled but would be expected to have a similar level of spectral density in the planned test compared to the sample data. By optimising the sensor locations and using sensors with a lower noise level in the main test, it would be expected that a larger SNR would be achievable.

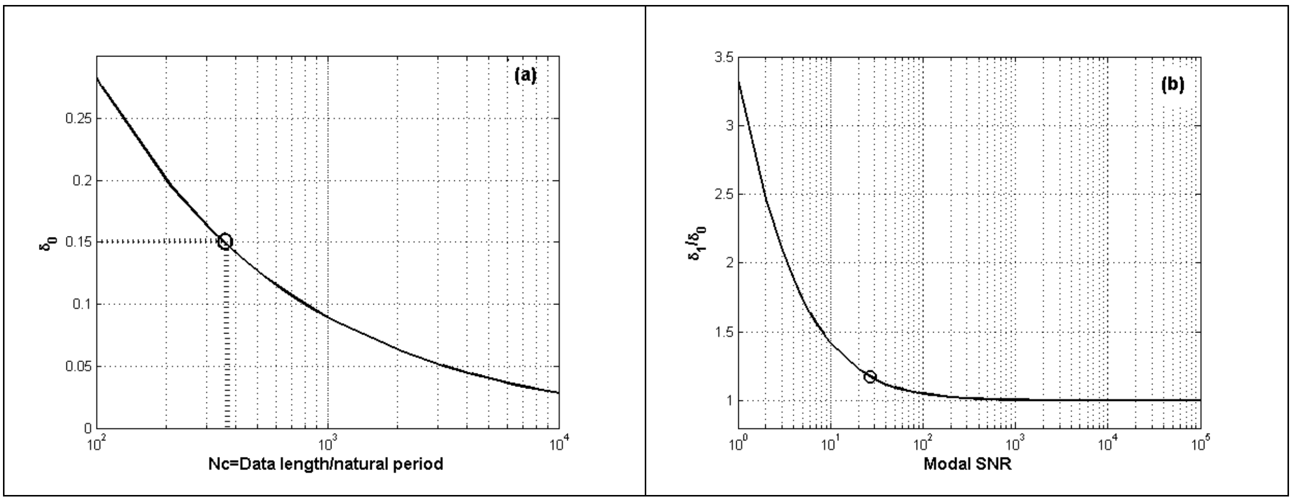

Figure 9: Zeroth and first order CoV. for damping ratio given parameters for Jiangyin Bridge first vertical mode. (a) zeroth order without effect of SNR, (b) first order correction depending on SNR.

4.2 Planning without preliminary data

It is reasonable to expect that MPs for Jiangyin Bridge would be similar to those obtained at Humber Bridge [31] and Fatih Mehmet Sultan Bridge [38] (B2, Turkey). The critical modes for each of these bridges are the fundamental lateral and vertical modes L1 and V1 and could be used in the absence of the JSTI sample data.

For B2, MP identified by 1st generation OMA are V1 (f=0.125 Hz, ζ=1.33%), L1 (f=0.077 Hz, ζ<14.4%), for the British bridge using 2nd generation OMA V1 (f=0.116 Hz, ζ=3.1%), L1 (f=0.055 Hz, ζ=4%).

Practical guidelines for planning ambient vibration tests for Bayesian OMA are given in [27]. Without preliminary data, MP for the similar bridges (i.e. Humber and B2) could be used to guide planning, although in this case natural frequency estimates are available, which are quite close to values for Humber and B2. Without other information on data quality the bandwidth factor κ is not known. To separate the effect of data duration and SNR, the first order posterior CoV. represented in equations (1) and (3) is rearranged into two factors:

$$\delta_1 = A_1 A_2$$

where

$$A_1 = \frac{1}{\sqrt{2\pi\zeta N_c}}$$

$$A_2 = \sqrt{\frac{1 + a(\kappa)/\gamma}{B(\kappa)}}$$

and $B(\kappa)$ and $a(\kappa)$ are given in equations (5) and (6).

Figure 10 shows A_1, which accounts for the duration (in terms of number of cycles) and A_2, which separately accounts for the SNR. At the planning stage the bandwidth factor κ is not known, but it can be taken to depend on the SNR [27] since a more noisy signal buries the spectral peak, reducing the useful frequency range of information. A reasonable choice consistent with common practice is the minimum of $2\sqrt{\gamma}$ and some $\kappa_{\max}$ that controls the risk of modelling error (e.g. unaccounted mode). Again, these considerations on the bandwidth factor are only relevant at the planning stage because its value directly results from the choice of the band for identification when the data is available.

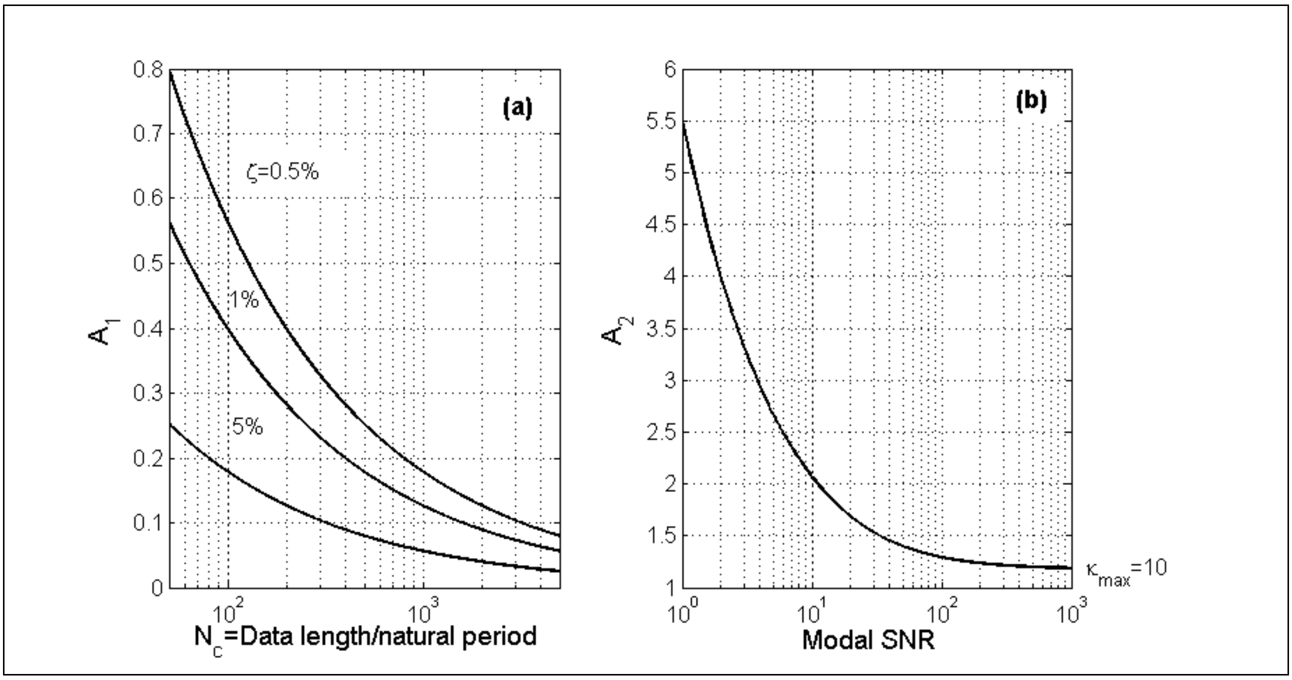

Figure 10: Assessing test configuration in terms of a) data duration and b) modal SNR.

Although a value of SNR=27 is available from preliminary data, a typical value could also be obtained using the accelerometer noise floor and the experience from other bridges. From the OCXO laboratory huddle test, the sensor and acquisition system background noise is $\sqrt{S_e}$=30 $\mu ms^{-2}/\sqrt{Hz}$, while the square root of modal acceleration PSD for the most challenging first lateral mode would be somewhere between the values obtained from the Humber Bridge, $\sqrt{S}/2\zeta$=0.007 $ms^{-2}/\sqrt{Hz}$, and B2, $\sqrt{S}/2\zeta$= 0.005 $ms^{-2}/\sqrt{Hz}$ (Figure 11), giving a worst case SNR=3×10^4, much better than from the preliminary data.

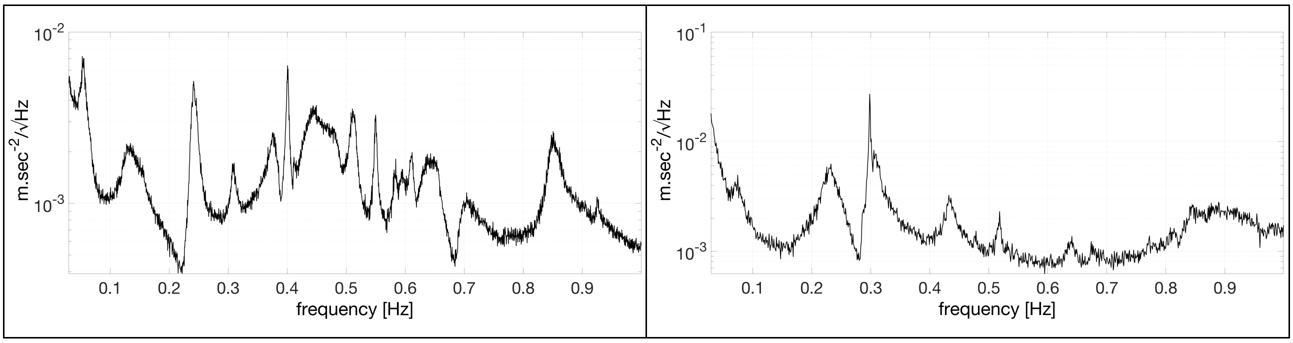

Figure 11: Square root PSD for Humber Bridge (left) and Second Bosporus Bridge (right) lateral acceleration.

4.3 Factors controlling modal SNR

Modal SNR derives from two factors. The quality of the sensor and data acquisition hardware control the noise PSD S_e while the number and location of sensors control modal force PSD S, which is proportional to the square of the mode shape values at the measured degrees of freedom (DOFs). For identifying a single mode with multiple sensors, the obviously strategy is to maximise the sum of squares of mode shape values.

Sensor locations on a structure (test points or TPs) will have up to three DOFs, and their locations will be chosen logically according to convenient structural features - for example, the hanger (suspender) attachment points to the deck. For all the referenced long span bridge AVTs tests there were more DOFs than available single-axis sensors. Reference TPs and DOFs are selected common to all setups so that mode shape pieces can be glued or assembled [46]. Therefore, for the purposes of planning a modal test, the questions to be answered are:

1. How many reference locations should be measured?
2. Where should the reference sensors be placed?
3. How should the remaining sensors be roved in how many setups?
4. How long should the data (acquisition) of each setup be?

Although there are possibilities, such as daisy chaining references, to simplify planning we assume that the reference location or locations are fixed in all setups. Reference sensors should be located so that the target modes, or as many modes as possible, can be identified in all setups, avoiding modes of interest while maximising modal responses (via mode shape ordinates) for expected mode shapes, which can be based on experience or numerical simulations.

So where are the best reference locations? Figure 12 shows a set of ten mode shapes for a simply supported beam with 41 TPs (indicated by vertical bars, including support locations). These mode shapes might resemble vertical mode shapes of a suspension bridge and siting a reference anywhere from the 5th to the 37th TPs will find at least one mode having modal ordinate at or close to zero. However, the first mode, which has the smallest modal ordinates in the TP ranges 2-4 and 38-40, is likely to be the most important to identify reliably. One possible strategy is to use multiple references, but this reduces the number of 'roving' sensors available for remaining test points, which will require more setups each using (for a fixed available test campaign duration) reduced data duration T.

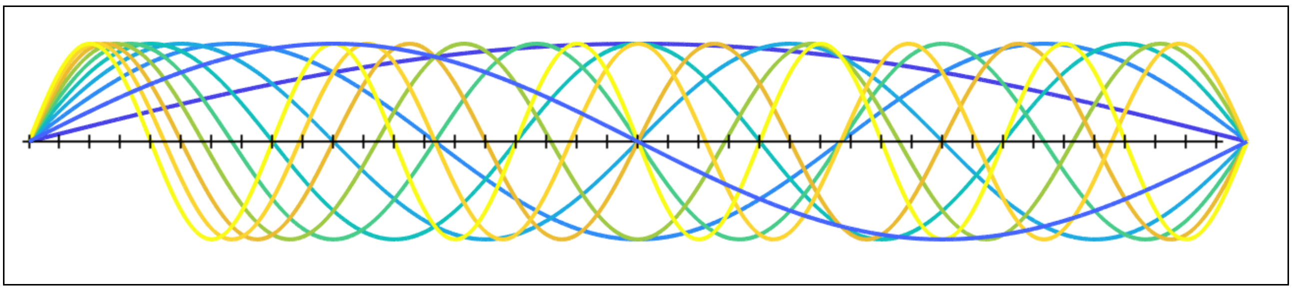

Figure 12: Ten mode shapes for a simply supported beam with 41 TPs.

For a single mode where the reference DOF ordinate is counted only once, maximising the SNR for the same modal excitation and sensor type means maximising the sum of squares of mode shape values. For the usual case of measuring multiple modes where the SNR is proportional to at least the square of the modal ordinate, there is as yet no metric to maximise.

5 Ambient vibration test (AVT)

The AVT was scheduled for Tuesday 25th to Thursday 27th April 2017. Equipment comprising four loggers, 12 QA-750 accelerometers, 240 m of colour-coded signal cable in 10 m and 20 m lengths and a laptop were flown from the UK as checked baggage, with NI hardware removed from the loggers and packed securely. A set of four high-capacity batteries were provided by JSTI and local transport was provided by JSTI. Weather was mostly fine, usually low visibility with smog clearing towards the end of the test, minimal rain and weak to moderate winds. The south end of the east walkway of the bridge was accessed by driving from the south and parking at the tower at the edge of the traffic lanes, then climbing onto the walkway from the approach span side. Hanger attachment points are clearly numbered from north to south, and the four channels of the master OCXO box were used as references with lateral (transverse direction) and vertical accelerometers at TP67 and TP71, aiming to identify mode shape pieces using three roving OCXO boxes, each typically measuring at a single TP. Figure 13 shows Jiangyin Bridge TPs, corresponding to hanger attachment points and tower portals, as well as indicating reference locations and TPs for a typical measurement setup.

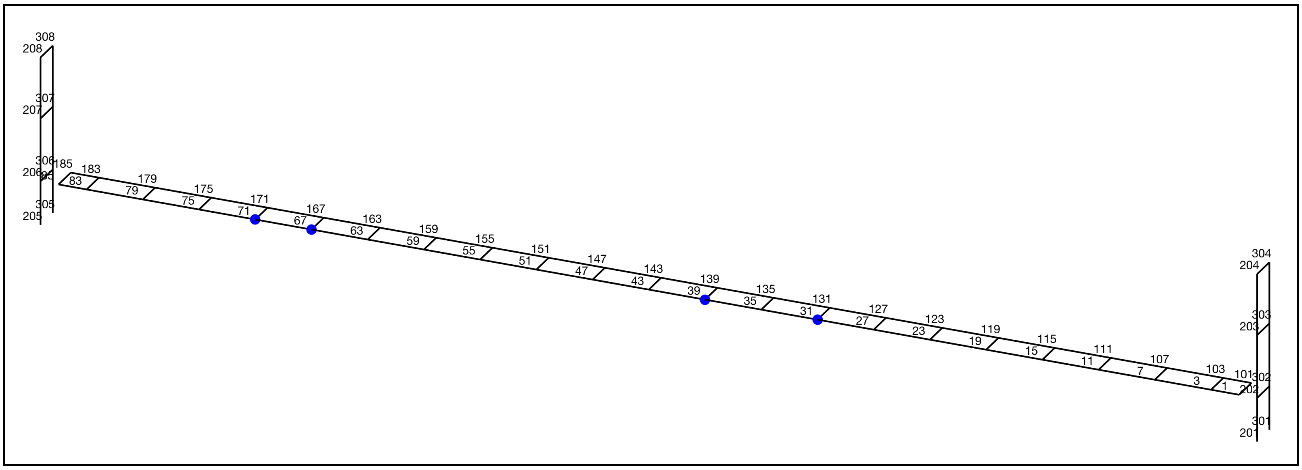

Figure 13: Jiangyin Bridge test points and sensor locations for a measurement setup.

A detailed method statement, including a risk assessment, was prepared for the scheduled three days comprising a sequence of one-hour measurements, with an option to use a fourth day in the event of bad weather. The plan covered every fourth TP on the east walkway, two TPs on the west walkway opposite the reference TPs, as many as possible TPs on the south tower, and if time permitted, the equivalent locations on the north tower. Figure 14 shows the loggers being synchronised before a huddle test at the start of the sequence and the pair of accelerometers at TP67. The bridge is aligned approximately in north-south axis with a coordinate system of X=longitudinal, positive to the north, Y=lateral, positive to the west and Z=vertical, positive upwards.

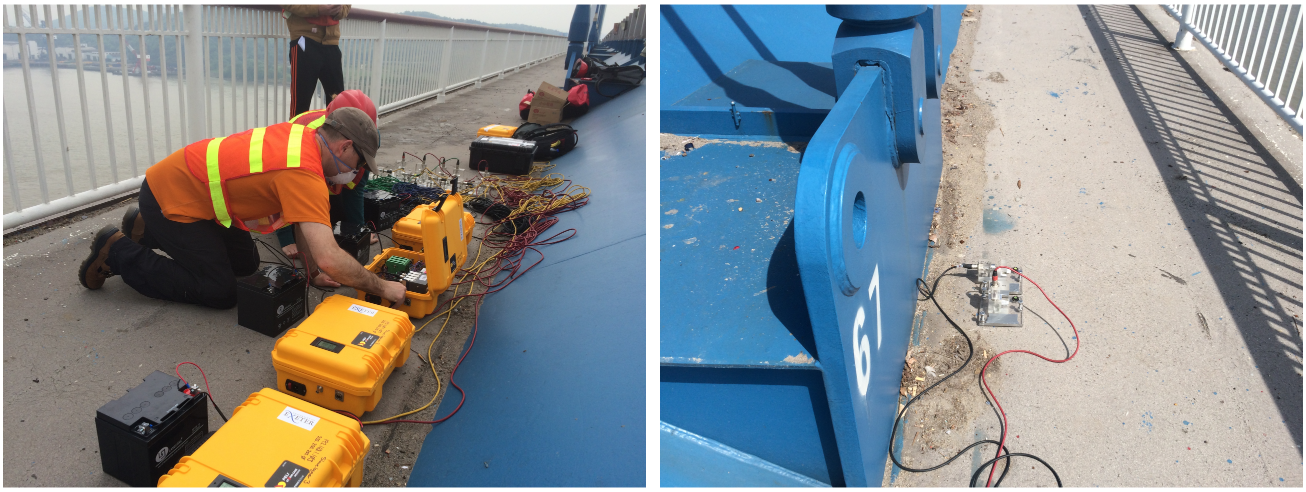

Figure 14: Setting up acquisition for initial huddle test and reference accelerometers at H67.

The reference accelerometer signals were recorded by the master logger continuously during the day of measurement while the three slave loggers were roved to remaining TPs. The moves were coordinated by mobile phone text messages and timed so as to maintain a minimum one hour recording for all loggers. Square root PSD plots for the first day of vertical and lateral acceleration data at TP67 are shown in Figure 15.

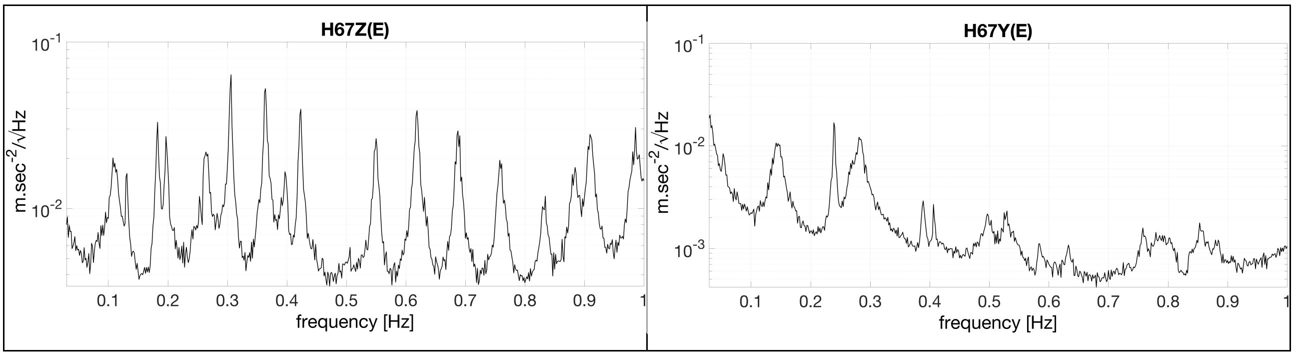

Figure 15: Sample square root PSD for TP67 vertical (Z) and lateral (Y) acceleration.

Table 1 Summarises the measurement sequence over three days.

Table 1: Measurement setup using two to four acquisition channels (ADs) of master and slave loggers.

setup	day	start	end	M				S1			S3		
				DA1	DA2	DA3	DA4	DA1	DA2	DA3	DA1	DA2	DA3
1	26	11:14	12:17	H67EZ	H67EY	H71EZ	H71EY	H83EZ	H83EY	-	H75EZ	H75EY	-
2	26	12:30	13:34	H67EZ	H67EY	H71EZ	H71EY	H63EZ	H63EY	-	H55EZ	H55EY	-
3	26	13:41	14:45	H67EZ	H67EY	H71EZ	H71EY	H51EZ	H51EY	-	H43EZ	H43EY	-
4	26	14:54	16:00	H67EZ	H67EY	H71EZ	H71EY	H39EZ	H39EY	-	H31EZ	H31EY	-
5	26	16:08	17:10	H67EZ	H67EY	H71EZ	H71EY	H27EZ	H27EY	-	H19EZ	H19EY	-
6A	27	10:19	11:20	H67EZ	H67EY	H71EZ	H71EY	H23EZ	H23EY	-	H15EZ	H15EY	-
6B	27	11:26	12:30	H67EZ	H67EY	H71EZ	H71EY	H35EZ	H35EY	-	H11EZ	H11EY	-
6C	27	12:36	13:38	H67EZ	H67EY	H71EZ	H71EY	H47EZ	H47EY	-	H7EZ	H7EY	-
6D	27	13:53	14:55	H67EZ	H67EY	H71EZ	H71EY	H59EZ	H59EY	-	H3EZ	H3EY	-
6E	27	15:02	16:05	H67EZ	H67EY	H71EZ	H71EY	H79EZ	H79EY	-	-	-	-
6F	27	16:12	17:13	H67EZ	H67EY	H71EZ	H71EY	H85EZ	H85EY	-	STLEX	STLEY	-
7	28	10:16	11:22	H67EZ	H67EY	H71EZ	H71EY	H71WZ	H71WY	-	H67WZ	H67WY	-
8	28	12:30	13:30	H67EZ	H67EY	H71EZ	H71EY	STUEX	STUEY	STUWX	STMEX	STMEY	STMWX

E/W are east/west side of bridge; L/M/U are lower/mid/upper portal levels of tower

Logger S2 was used in the first day of measurements but when data were merged it was found that synchronisation had not been correctly initiated. This was due to allowing too short a time for the synchronisation, requiring only a minor change in the initialisation procedure. An inelegant method to guard against this would be to generate a similar and obvious signal on all sensors while collocated at the start of the sequence after initialisation. An example would be a sequence of 'heel drops' on the bridge deck, providing obvious signals that could be subsequently aligned using correlations between data channels.

In this case, being the first major exercise, no chances were taken and measurements covered by S2 were repeated in setups 6A-6F, while S2 was not used until it could be thoroughly checked on return to the UK. Setup 6F included X and Y measurement of the south tower (ST) lower (L) portal, deck level east side (Figure 16 left) and setup 7 was designed to identify torsional modes.

Setup 8, with measurements in the middle and upper portal, was designed to characterise the tower component of deck girder modes as well as modes only involving the tower. Jiangsu Yangtze Bridge Co. provided access to the south tower via the door visible in Figure 16 (left), and the middle portal (interior shown in Figure 16 right reflecting the depth visible in Figure 2) was accessed by a lift. Access to the upper portal was via transfer to a second lift at a mezzanine level and to the top of the portal for the view of Figure 2 by staircase. The value of autonomous loggers was proven by the lack of GPS or wireless signal reception inside the middle portal, and it was more convenient to measure the inside the upper portal.

Figure 16: Measurements at lower (left) and middle (right) portal levels

6 Modal parameter estimates using Baysian operational modal analysis

To visualise the modes of interest and the relevant frequency bands, the (root) PSD spectrum of Setup 1 (as a typical case) is shown in Figure 17. It can be seen that the lines plotted in the PSD spectrum are generally separated into two levels, indicating two different PSD levels of modal responses among the data channels. The higher levels are those measuring vertical directions and the lower ones are those measuring lateral directions. This is a typical case for AVT of long-span bridges as the spectral density of modal forces in the vertical direction (mainly due to traffic) is normally much larger than those in the lateral direction (mainly due to wind). With this situation, it is easier to detect potential modes based on the PSD spectrum than on the singular value (SV) spectrum. This issue will also cause problems in identifying the lateral modes, which will be discussed later.

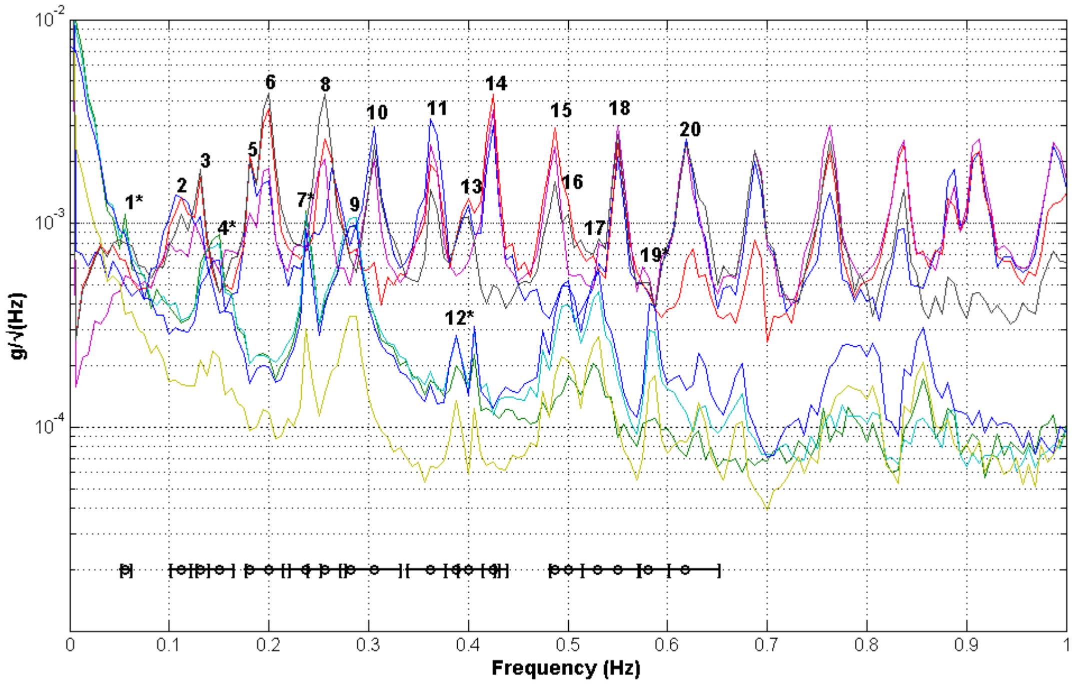

Figure 17: Square root PSD spectrum of Setup 1

There are many modes within the 0-1 Hz band, including several closely-spaced modes, which increases the identification difficulties and the associated uncertainty. Modal identification here focuses on the first twenty modes indicated in the PSD spectrum. The initial guesses of natural frequency and the selected frequency bands for modes of interest are indicated in the figure with symbols ‘o’ and ‘[-]’, respectively. The symbol ‘*’ (as the superscript) denotes that the mode is identified using data in the lateral direction only. Modal parameters are identified in individual setups based on the Bayesian FFT method [47,48] and the overall mode shapes are assembled using the global least square method [46]. In this procedure, the real parts (or projections on to real axes) of the mode shape ordinates are used, so the small phase angle shifts suggested earlier would have no consequence.

Table 2 summarises the representative values of the identified modal parameters and associate uncertainties, where the MPV (most probable value) in the table denotes the sample mean of MPVs among the setups and the CoV. CoV is calculated based on the representative variance (i.e., sum of sample variance among the setups and the sample mean of the posterior variance among the setups).

Table 2: Identification results (L: lateral; V: vertical; T: torsional; S: symmetric; A: antisymmetric; U: unsymmetrical)

Mode	Characteristic	Natural Frequency		Damping Ratio	
		MPV (Hz)	CoV (%)	MPV (%)	CoV (%)
1	L-1-S	0.0536	3.56	4.32	88.2
2	V-1-A	0.1095	1.17	4.88	40.6
3	V-2-S	0.1304	0.54	1.41	53.6
4	L-2-A	0.1434	0.68	3.78	28.1
5	V-3-S	0.1828	0.48	1.50	68.2
6	V-4-A	0.1971	0.32	0.91	34.3
7	L-3-U	0.2393	0.61	0.49	75.0
8	V-5-S	0.2560	1.03	0.98	45.8
9	T-1-S	0.2811	0.50	1.61	25.0
10	V-6-A	0.3044	0.31	0.97	48.2
11	V-7-S	0.3638	0.16	0.61	25.5
12	L-4-A	0.3896	0.34	1.63	57.3
13	V-8-S	0.3974	0.45	0.83	29.6
14	V-9-A	0.4227	0.11	0.41	37.8
15	V-10-S	0.4854	0.17	0.50	29.2
16	T-2-A	0.4995	0.45	1.29	27.7
17	T-3-A	0.5236	0.69	1.67	34.2
18	V-11-A	0.5499	0.16	0.54	31.2
19	L-5-A	0.5865	0.21	0.64	35.4
20	V-12-S	0.6185	0.18	0.50	28.3

Figure 18 shows the assembled global mode shapes of the modes identified in Table 2.

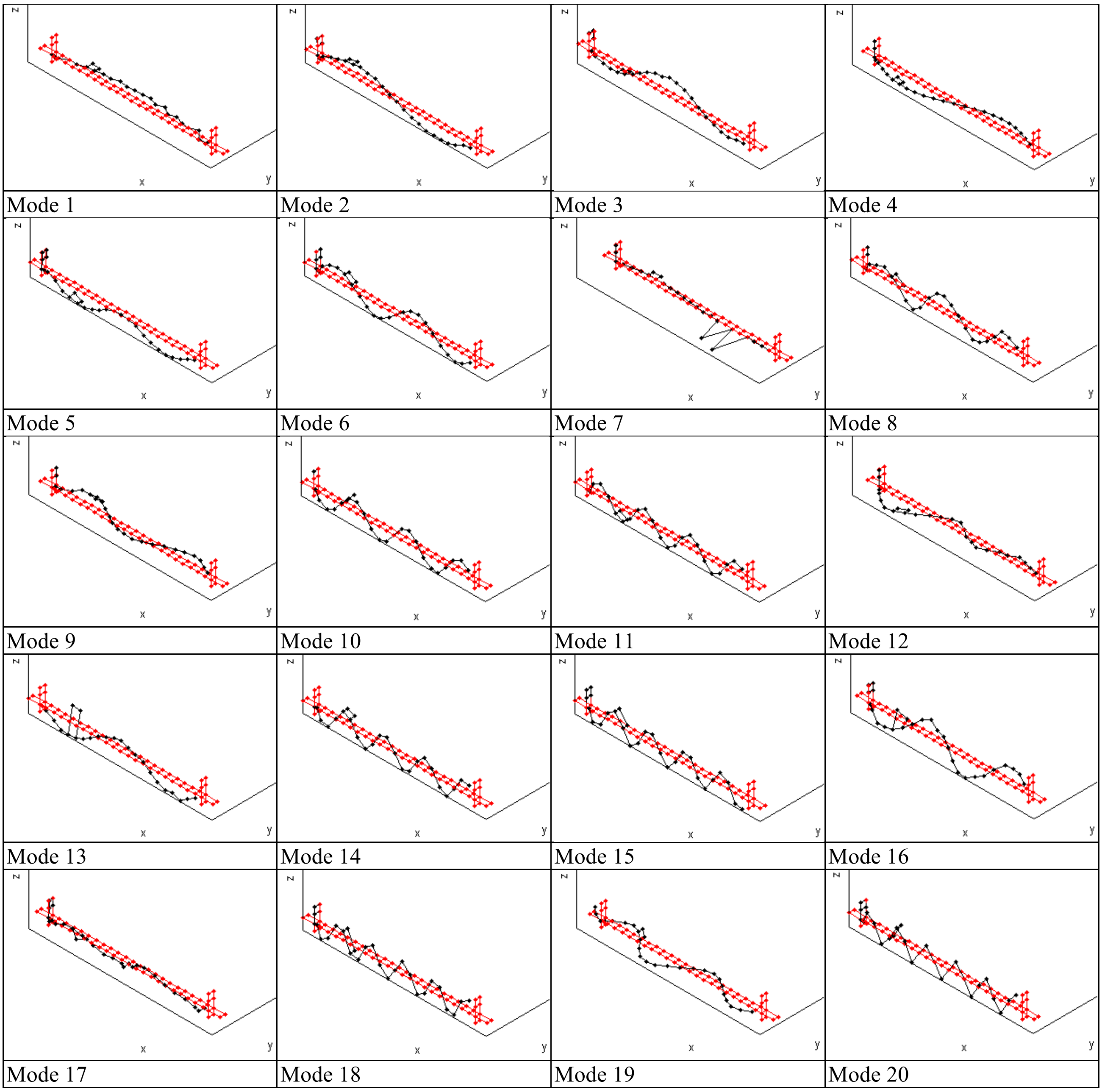

Figure 18: Identified global mode shapes

The first mode is a symmetric lateral mode with a natural frequency of 0.0536Hz, which is quite close to the value reported in the Chinese paper [34]. However, this mode cannot be identified based on the preliminary data (modal SNR is no better than unity), due to the high measurement noise in the low frequency range, meaning that the spectral peaks for this mode are not significant even in this AVT. It can be seen that there is an increase of the PSD in the frequency range lower than 0.1 Hz which derives from the measurement noise of the sensors as well as from the quasi-static rotation. The rotation appears as a DC offset of the signal and, along with the noise, overlays the modal contribution of the mode.

Spectral peaks cannot even be detected in some of the data channels in the vertical direction, which cause convergence problems in the modal identification procedure when all the data channels are involved for inference. In view of this, only the measured data in the lateral direction are used for Mode 1 identification and the overall mode shape is assembled assuming zero mode shape values in the vertical direction. Figure 19 shows the identified natural frequencies and damping ratios of Mode 1 among the setups, where the error bar represents ± posterior standard deviation of the identified MP. Large variations in the identified damping ratio can be found for Setup 6E and 7, which raise the overall identification uncertainty.

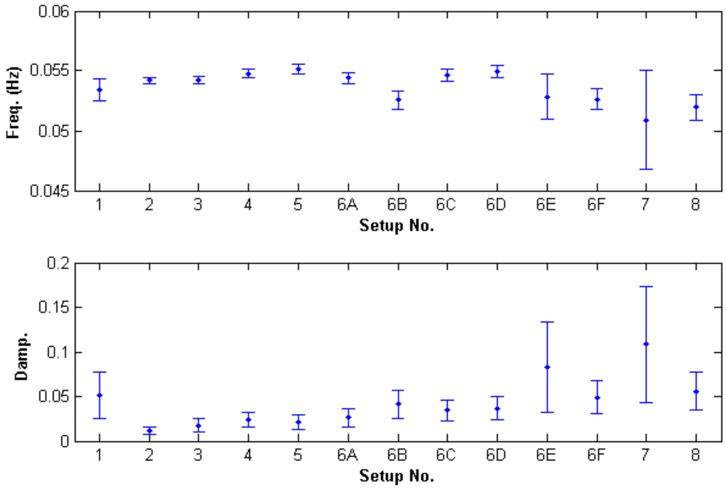

Figure 19: Identified natural frequency and damping ratio among the setups, Mode 1. (dot: MPV; errorbar: ± posterior standard deviation)

To illustrate the effect of modal SNR, Figure 20 shows the CoV. ratio δ_1/δ_0 for the posterior damping ratio of Mode 1. The circles reflect the identification uncertainty based on the current test configuration and the curves denote the value for each setup predicted by uncertainty laws. The values in the legend denote the CoV. of damping ratio quantified based on the measured data. It can be seen that all the setups lie in the low SNR region, where further increases in SNR can reduce the identification uncertainty by 30%.

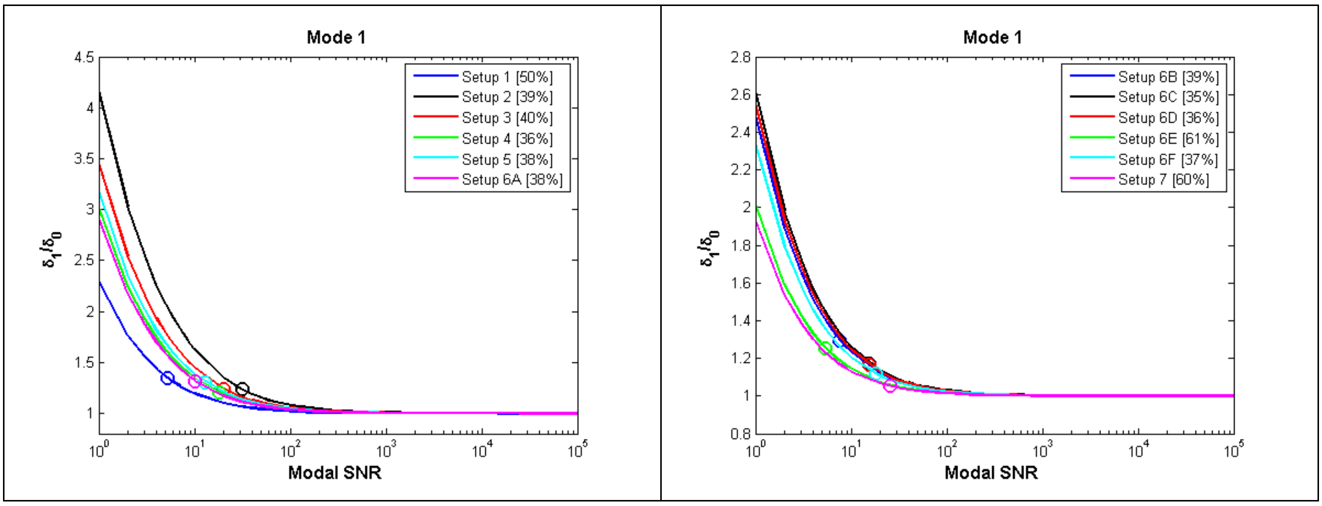

Figure 20: SNR effect with damping CoV., Mode 1 (left: Setup 1 to Setup 6A; right: Setup 6B to Setup 7)

The first vertical mode (Mode 2) is antisymmetric, with a natural frequency of 0.1095Hz. This is the mode corresponding to the one identified in the preliminary data for test planning. Figure 21 shows the CoV. ratio δ_1/δ_0 for posterior damping ratio of this mode. The posterior CoVs of damping ratio (as shown in the legend) are higher than the targeted value (i.e. 15%) in test planning. This is reasonable as the zeroth order uncertainty law used for the measurement duration plan assumes infinite SNR. The SNR of this mode varies among the setups, all are higher than the ~unity value for preliminary data, and they are close to the flat region of the predicted δ_1/δ_0 curve. Further increasing SNR will provide significant help in reducing the identification uncertainty, confirming the effectiveness of BAYOMALAW for planning.

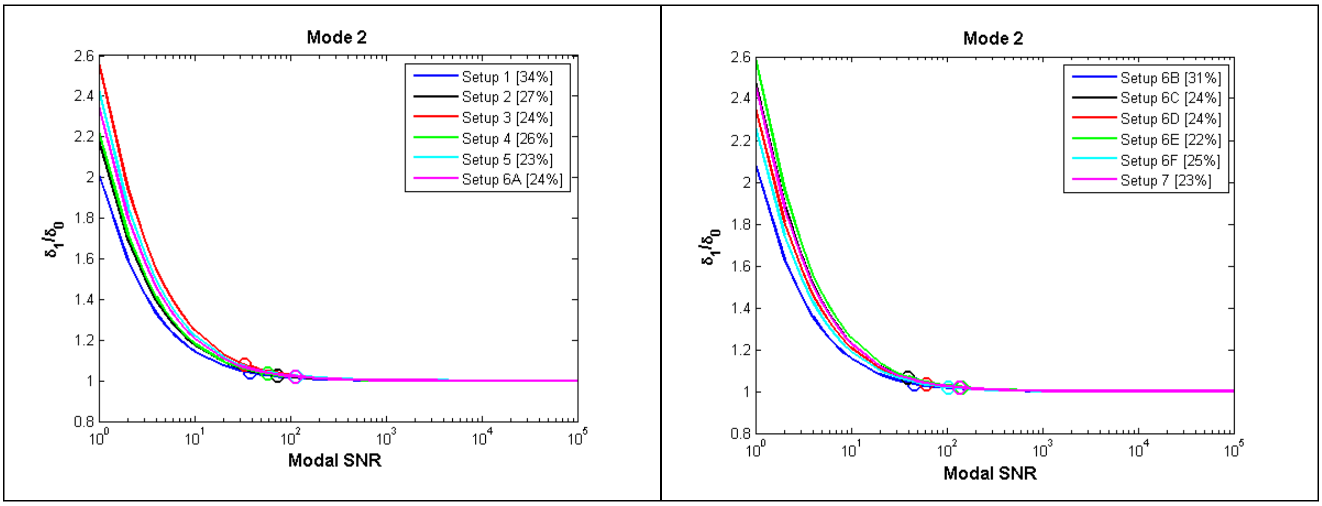

Figure 21: SNR effect with damping CoV., Mode 2 (left: Setup 1 to Setup 6A; right: Setup 6B to Setup 7)

Within the resonance band of Mode 4 (lateral mode), large contributions are found from Modes 2 and 3 (both are vertical modes). Similar situations can be found for Mode 7, 12 and 19. Identifying these modes within their resonance frequency bands by assuming a single mode is not feasible, as the modal contribution of other modes in the bands are not negligible and sometimes even larger than the mode to be identified. On the other hand, selecting a wide band involving the nearby modes and identifying them simultaneously will increase the modelling error risk due to non-structural components within the band, as these modes may not be closely spaced. It turns out that the identification procedure cannot converge or provide a reasonable estimation on the modal parameters of these modes. In view of this, these modes (i.e., Modes 4, 7, 12 and 19) are identified within their resonance frequency band using data channels in the lateral direction only to eliminate the effect of nearby modes. The mode shape values in the vertical direction are assumed to be zero when assembling the overall mode shapes.

The identified mode shape of Mode 7 in Setup 5 is peculiar because of two anomalous large ordinates. The cause is evident from Figure 22, showing the PSD spectrum of Setup 5 where there are additional peaks in the selected frequency band for Mode 7. The mode shape values are erroneously identified due to these peaks, which may not refer to a global mode as they cannot be found in other setups. To avoid their effect, modal identification has been conducted for mode 7 with a narrower frequency band where the additional peaks are not involved. Figure 23 shows the identified mode shapes, which now look more reasonable.

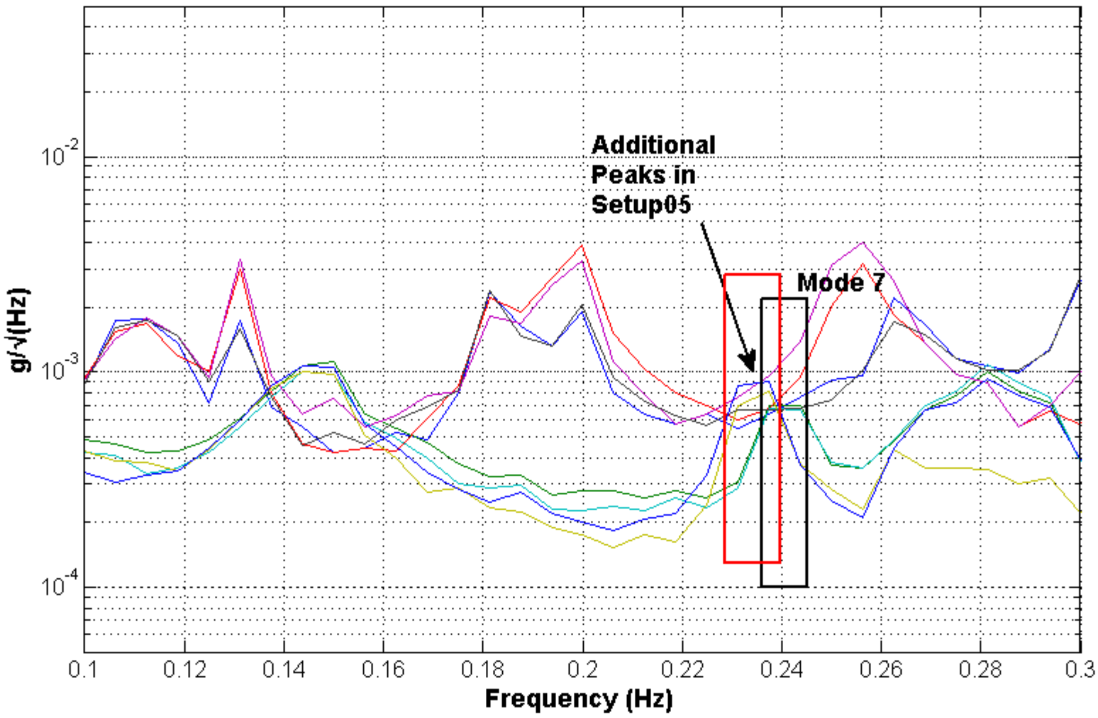

Figure 22: Square root PSD spectrum of Setup 5.

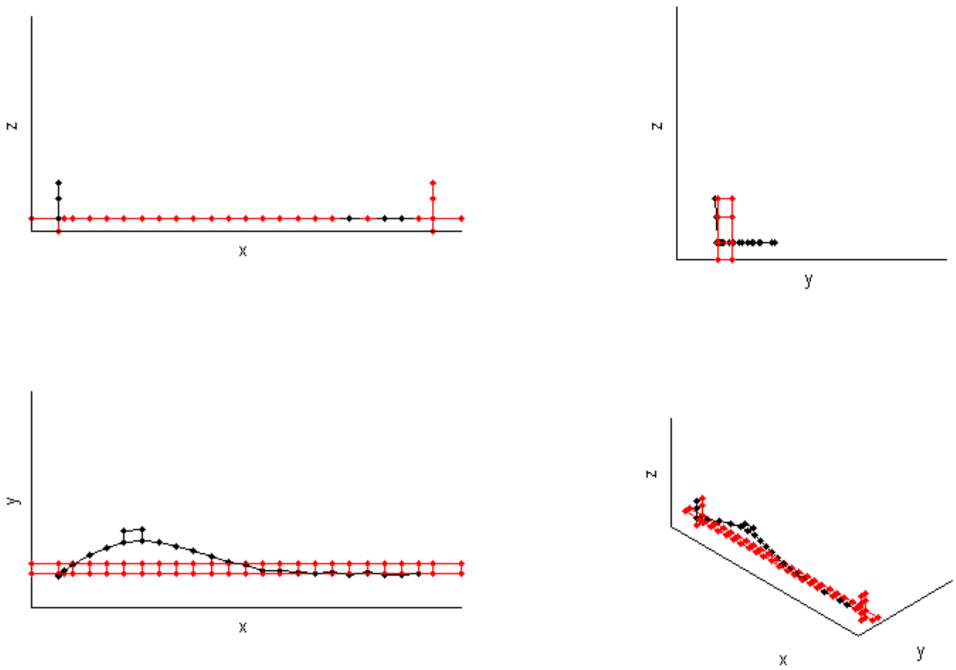

Figure 23: Overall mode shape of Mode 7 identified based on the narrower band

Thanks to the setup on the east side of the deck (i.e., Setup 7), torsional modes can be detected and identified. Specifically, Mode 9 is identified as a symmetric torsional mode and Modes 16 and 17 are antisymmetric torsional modes. Some torsional modes may be erroneously counted as lateral modes in this test as some modes are identified using data channels in the lateral direction only where the mode shape values in the vertical direction are not identified.

7 Discussion and conclusions

Modal tests of long span (suspension) bridges are among the most challenging of all types of field measurements due to their scale and to (as far as the authors know) the lowest frequencies observed in any man-made structure. Reliable MP identification, particularly of fundamental vertical and lateral mode damping ratios has been compromised by both bias errors introduced by early (first generation) OMA procedures and the large variance errors that appear to reduce only by using extremely long measurement periods, trading off stationarity properties of signals and environmental influence on structural properties. The question has always been how long a data record is necessary, what quantity and quality of equipment is adequate, and what level of accuracy can be achieved. Now it is possible to define a level of accuracy and determine the best measurement configuration in terms of sensor type, location and measurement duration in order to achieve it.

Then, if mode shapes are required to completely define the mode, how should they be best constructed using resources available and how to get around the difficulty of synchronising acquisition at locations separated by distances of the order of 1 km without constraint of cables, or the need to receive radio signals from satellites (GPS) or other loggers (by radio) for synchronisation?

These challenges have been addressed in a single exercise, with the bonus of a rare collaboration with Chinese researchers allowing a foreign team access to test a Chinese bridge.

The decision to use an hour of data for each measurement appeared optimal from the point of view of MP uncertainty and allowing for sufficient setups to define the global modal characteristics. It was not believed to be necessary to measure both sides of the bridge completely due to the single measurement on the west side and symmetry about the longitudinal axis.

However, the bridge may not be symmetric about the mid span, as indicated by lateral modes 7 and 12, so it cannot be assumed that lateral mode participation of the north tower would be identical to that of the south tower. Experience with suspension bridge towers e.g. [38] has shown that in addition to participating in deck modes driven by the cables, they have their own set of modes consistent with a cantilever having fixity at the freer end depending on the cable detail and back span arrangement.

The combination of sensor and data acquisition systems gives rise to background noise $S_{e,}$ which is adequate for the purpose, judging by the SNR of the acquired data (Figure 20, Figure 21). In fact, good enough SNR would be obtained for fundamental modes even with reference sensors much closer to the tower, where the mode shape ordinates are much reduced. This would mean less chance of locating at the nodal point of a high frequency mode and possibly negating the need for a backup reference location. Other sensor options would be to use JA-70SA or Guralp CMG5T units, both low-noise tri-axial devices, but while single axis sensors might be more cumbersome and require more local wiring, they offer more flexibility.

Based on the experience, to obtain the most useful planning data, the authors would recommend a preliminary measurement using a single logger and small set of uniaxial accelerometers laid out close to the tower of a long span bridge, aligned first vertically then laterally. This would provide enough information to characterise the signal to noise ratio of the fundamental modes and determine an appropriate setup duration. It would also qualify the use of a reference location close to a tower.

8 Acknowledgements

The research was funded by the Engineering and Physical Sciences Research Council (grant EP/N017897/1 and EP/N017803).

We are very grateful to: Prof. Jun Chen of Tongji University for logistical assistance; to Dr Vincent Ao for help designing the OCXO logger system; to Dr Ki Koo for evaluating the OCXO clock performance; to Ms Karen Faulkner for her participation in the site activities; to the JSTI driver who ferried the UK AVT team (Bassitt/Brownjohn/Faulkner/Zhu) around Jiangsu Province.

References

[1] F.N. Catbas, T. Correa-Kijewski, A.E. Aktan, Structural Identification of Constructed Systems. Approaches, Methods and Technologies for Effective Practice of St-Id., ASCE, 2013.

[2] J.M.W. Brownjohn, E.P. Carden, C.R. Goddard, G. Oudin, Real-time performance monitoring of tuned mass damper system for a 183m reinforced concrete chimney, J. Wind Eng. Ind. Aerodyn. 98 (2010) 169–179.

[3] J.M.W. Brownjohn, K.Y. Koo, C. Basagiannis, A. Alskif, A. Ngonda, Vibration monitoring and condition assessment of the University of Sheffield Arts Tower during retrofit, J. Civ. Struct. Heal. Monit. (2013)..

[4] E.J. Cross, K.Y. Koo, J.M.W. Brownjohn, K. Worden, Long-term monitoring and data analysis of the Tamar Bridge, Mech. Syst. Signal Process. 35 (2013) 16–34.

[5] J.M.W. Brownjohn, T.-C. Pan, Response of tall buildings to weak long distance earthquakes, Earthq. Eng. Struct. Dyn. 30 (2001) 709–729.

[6] S. Lagomarsino, Forecast models for damping and vibration periods of buildings, J. Wind Eng. Ind. Aerodyn. 48 (1993) 221–239.

[7] M.R. Willford, R. Smith, R. Merello, Intrinsic and supplementary damping in tall buildings, Proc. ICE - Struct. Build. 163 (2010) 111–118.

[8] A. Kareem, K. Gurley, Damping In structures: Its evaluation and treatment of uncertainty, J. Wind Eng. Ind. Aerodyn. 59 (1996) 131–157.

[9] ESDU, Damping of structures. Part 1: tall buildings, ESDU, 1983.

[10] T. Kijewski-Correa, A. Kareem, On the reliability of a class of system identification techniques: insights from bootstrap theory, Struct. Saf. 24 (2002) 261–280.

[11] D.J. Ewins, Modal Testing: Theory, Practice and Application, Research Studies Press Ltd., Baldock, Hertfordshire, England, 2000.

[12] B. Peeters, G. De Roeck, Stochastic system identification for operational modal analysis: A review, J. Dyn. Syst. Meas. Control. 123 (2001) 659–667.

[13] R. Brincker, L. Zhang, P. Andersen, Modal identification of output-only systems using frequency domain decomposition, Smart Mater. Struct. 10 (2001) 441–445.

[14] L.C. Pagnini, Serviceability criteria for wind-induced acceleration and damping uncertainties, J. Wind Eng. Ind. Aerodyn. 74 (1998) 1067–1078.

[15] M.D. Burton, K.C.S. Kwok, A. Abdelrazaq, Wind-induced motion of tall buildings: Designing for occupant comfort, Int. J. High-Rise Build. 4 (2015) 1–8.

[16] T. Kijewski-Correa, J. Kilpatrick, A. Kareem, D.K. Kwon, B. Bashor, M. Kochly, et al., Validating wind-induced response of tall buildings: Synopsis of the Chicago full-scale monitoring program, ASCE J. Struct. Eng. 132 (2006) 1509–1523.

[17] A.G. Davenport, G.L. Larose, The structural damping of long span bridges: An interpretation of observations, in: Canada-Japan Work. Bridg. Aerodyn., 25–27 Sept ed., NRC Canada, Ottawa, 1989: pp. 1–7.

[18] J.M.W. Brownjohn, Estimation of damping in suspension bridges, Proc. ICE - Struct. Build. 104 (1994) 401–415.

[19] S.K. Au, Y.-C. Ni, Fast Bayesian modal identification of structures using known single-input forced vibration data, Struct. Control Heal. Monit. 21 (2014) 381–402.

[20] P. Mellinger, M. Döhler, L. Mevel, Variance estimation of modal parameters from output-only and input/output subspace-based system identification, J. Sound Vib. 379 (2016) 1–27.

[21] R. Pintelon, P. Guillaume, J. Schoukens, Uncertainty calculation in (operational) modal analysis, Mech. Syst. Signal Process. 21 (2007) 2359–2373.

[22] E. Reynders, R. Pintelon, G. De Roeck, Uncertainty bounds on modal parameters obtained from stochastic subspace identification, Mech. Syst. Signal Process. 22 (2008) 948–969.

[23] M. Döhler, X.-B. Lam, L. Mevel, Uncertainty quantification for modal parameters from stochastic subspace identification on multi-setup measurements, Mech. Syst. Signal Process. 36 (2013) 562–581.

[24] S.K. Au, F.-L. Zhang, Y.-C. Ni, Bayesian operational modal analysis: Theory, computation, practice, Comput. Struct. 126 (2013) 3–14.

[25] J.L. Beck, Bayesian system identification based on probability logic, Struct. Control Heal. Monit. 17 (2010) 825–847.

[26] S.K. Au, J.E. Mottershead, J.M.W. Brownjohn, Uncertainty Quantification and Management in Ambient Modal Identification, EPSRC Grants Web (2016).

[27] S.K. Au, J.M.W. Brownjohn, J.E. Mottershead, Quantifying and managing uncertainty in operational modal analysis, Mech. Syst. Signal Process. 102 (2018) 139–157.

[28] R. Brincker, C.E. Ventura, Introduction to Operational Modal Analysis, John Wiley & Sons, Ltd, Chichester, UK, 2015.

[29] S.K. Au, Uncertainty law in ambient modal identification - Part I: Theory, Mech. Syst. Signal Process. 48 (2014) 15–33.

[30] S.K. Au, Uncertainty law in ambient modal identification---Part II: Implication and field verification, Mech. Syst. Signal Process. 48 (2014) 34–48.

[31] J.M.W. Brownjohn, F. Magalhães, E. Caetano, A. Cunha, Ambient vibration re-testing and operational modal analysis of the Humber Bridge, Eng. Struct. 32 (2010) 2003–2018.

[32] J. Young, Jiangyin Yangtze River Bridge, China, Proc. Inst. Civ. Eng. - Bridg. Eng. 156 (2003) 45–53.

[33] Q. Xia, J. Zhang, Y. Tian, Y. Zhang, Experimental Study of Thermal Effects on a Long-Span Suspension Bridge, J. Bridg. Eng. 22 (2017).

[34] Y. Zhang, C. Zhang, Y. Cheng, X. Chen, Y. Fan, Dynamic characteristic analysis of the Jiangyin Yangtze River Highway Bridge based on GPS technology, Highw. (in Chinese). 2 (2010) 5–7.

[35] Z. Sun, Y. Zhang, Failure mechanism of expansion joints in a suspension bridge, J. Bridg. Eng. 21 (2016) 1–13.

[36] J.D. Littler, J.M.W. Brownjohn, Ambient vibration measurements of the Humber suspension bridge and comparison with calculated characteristics -discusson, Proceeding Inst. Civ. Eng. Part 2. 85 (1988) 728–730.

[37] J.M.W. Brownjohn, A.A. Dumanoglu, R.T. Severn, A.B. Blakeborough, Ambient vibration survey of the Bosporus suspension bridge, Earthq. Eng. Struct. Dyn. 18 (1989) 263–283.

[38] J.M.W. Brownjohn, A.A. Dumanoglu, R.T. Severn, Ambient vibration survey of the Fatih Sultan Mehmet (Second Bosporus) Suspension Bridge, Earthq. Eng. Struct. Dyn. 21 (1992) 907–924.

[39] J.M.W. Brownjohn, A. Pavic, E.P. Carden, E.P., Middleton, C.J., Modal testing of Tamar suspension bridge, in: IMAC XXV, Orlando, Orlando, USA, 2007.

[40] K.Y. Koo, J.M.W. Brownjohn, D.I. List, R. Cole, Structural health monitoring of the Tamar Suspension Bridge, Struct. Control Heal. Monit. 20 (2012) 609–625.

[41] K.Y. Koo, J.J. Lee, J.M.W. Brownjohn, Time synchronisation for wireless sensors by using low-cost GPS module, in: Proceedings, 7th Int. Conf. Struct. Heal. Monit. Intell. Infrastruct., Turin, 2015: pp. 1–8.

[42] Guralp, MAN-RTM-0003 - Real-time Clock Operator’s Guide, (2016).

[43] J.M.W. Brownjohn, S.K. Au, B. Li, J. Bassitt, Optimised ambient vibration testing of long span bridges, in: EURODYN 2017, Elsevier, Rome, 2017: p. 10.

[44] S.K. Au, Operational Modal Analysis: Modeling, Bayesian Inference, Uncertainty Laws, Springer,

2017.

[45] R. Sleeman, Three-channel correlation analysis: A new technique to measure instrumental noise of digitizers and seismic sensors, Bull. Seismol. Soc. Am. 96 (2006) 258–271.

[46] S.K. Au, Assembling mode shapes by least squares, Mech. Syst. Signal Process. 25 (2011) 163–179.

[47] S.K. Au, Fast Bayesian ambient modal identification in the frequency domain, Part I : Posterior most probable value, Mech. Syst. Signal Process. 26 (2012) 60–75.

[48] S.K. Au, Fast Bayesian ambient modal identification in the frequency domain, Part II: Posterior uncertainty, Mech. Syst. Signal Process. 26 (2012) 76–90.